Engineering Conferences International
ECI Digital Archives

The 14th International Conference on Fluidization – From Fundamentals to Products

Refereed Proceedings

2013

Development of a Novel Infrared Camera for Gas Exchange from Bubble-to-Emulsion Phase in Gas-Solid Fluidized Beds

Nhi Dang
Eindhoven University of Technology, Netherlands

Tom Kolkman
Eindhoven University of Technology, Netherlands

Fausto Gallucci
Eindhoven University of Technology, Netherlands

Martin van Sint Annaland
Eindhoven University of Technology, Netherlands

DEVELOPMENT OF A NOVEL INFRARED CAMERA FOR GAS EXCHANGE FROM BUBBLE-TO-EMULSION PHASE IN GAS-SOLID FLUIDIZED BEDS

Nhi Dang*, Tom Kolkman , Fausto Gallucci and Martin van Sint Annaland
Eindhoven University of Technology; Dept. Chemical Engineering and Chemistry
PO Box 513, 5600 MB Eindhoven, The Netherlands
E*: t.y.n.dang@tue.nl

ABSTRACT
Gas exchange from bubble-to-emulsion phase has been measured by the development of a novel infrared camera combined with a visual high speed camera and the Digital Image Analysis, non-invasively. Experimental findings indicate that the concentration inside the bubble is non-uniform and being diluted at the bottom and in the centre of the bubbles. The gas exchange coefficient is determined from the single phase model and dominated by the convective flow.

Keywords: Bubble-to-emulsion phase, Infrared camera, Digital Image Analysis, Gas exchange rate.

INTRODUCTION
Gas exchange between the gas-solids phase occurs via the combined effects of gas diffusion, coherent gas flow and solids motion carrying adsorbed gas atoms (1-3). Experiments of bubble-to-emulsion phase gas exchange generally used invasive technique by injecting bubbles containing a tracer gas into incipiently fluidized bed and the concentration of the tracer gas was measured either in the emulsion phase or at the outlet of the bed (4-7). The invasive probes disturb the flow path of the bed operation, while the injected bubbles differs significantly from generated bubbles in terms of size, density and dynamics. Recent developments are based on the imaging techniques like X-ray (8), MRI (9) which have allowed non-intrusive and fast measurements of flow behaviours. Pavlin et al., 2007 [10] applied MRI technique to measure the mass transfer from bubble to emulsion phase in gas-solids fluidized bed using laser-polarized xenon (^{129}Xe). However, the MRI technique is limited by an extremely high investment cost and the required particles containing MR-sensitive nuclei.

To the best of the authors' knowledge, the gas exchange from bubble-to-emulsion fluidized bed has never been investigated visually due to the opaque systems and the transparency of tracer gases (like CO_2, He). It is thus the gas streamlines the concentration profile as well as the (back) mixing flow may have not been well interpreted. All models' descriptions in literature (1, 11) are based on the uniform concentration profile, constant bubble size and bubble rise velocity assumptions. However, Patil et al., (6) applied CFD simulation and stated that the concentration inside the bubble is non-uniform that is lower in the centre and at the bottom part of the bubbles. To precisely quantify the mass exchange rate in the fluidized bed system; the transportation mechanism, the gas flow pattern as well as the concentration distribution inside the bubble are of great importance.

This study develops a rapid novel experimental technique using Infrared Camera with a proper optical filter centred on IR absorbing wavelength of a tracer gas, to measure the gas-solids interchange in a thin fluidized bed, non-invasively. In the present study, the characterization of the IR camera technique has been addressed, by designing a dedicated experimental setup for CO_2 concentration measurement. It has been started by the calibration procedure performed in the gas phase. Subsequently, the technique is extended into gas-solids fluidized beds for gas exchange rate from bubble-to-emulsion phase. The tracer gas concentration profiles inside the bubbles, the influence of bubble diameter as well as the particle size on the gas exchange coefficient have fully been investigated.

QUANTITATIVE ANALYSIS

The stretching vibration of CO_2 is asymmetric and produces a dipole moment, which oscillates with the vibrational frequency and is active in the infrared. This results in absorption at 4.26 μm (2350 cm^{-1}). Additionally, the bending motion also gives a dipole moment, corresponding to an absorption band at 15 μm (667cm^{-1}) ([12]). In this work, a narrowband optical filter for CO_2 has been used in front of the IR camera detector that allows CO_2 to be filtered at 4.26 μm wavelength.

The signal generated by the camera when a sapphire column flushed with nitrogen is placed in between the IR source and the camera, is indicated with DL_0. When CO_2 is fed into the column, it absorbs part of the radiation and the remaining signal transmitted to the camera is denoted with DL. From these two signals the transmittance and absorbance can be defined as:

$$T = \frac{DL}{DL_0} \tag{1}$$

$$A = -\ln \frac{DL}{DL_0} \tag{2}$$

The absorbance is in theory linear to the CO_2 concentration according to Lambert Beer's law:

$$A = -\varepsilon l C = aC \tag{3}$$

Where C = concentration [$mol.l^{-1}$], ℓ = target length [cm], ε: molar absorbance [$mol^{-1}.cm^{-2}$] and a is a function of l and ε.

However, the linear relationship between absorbance and concentration is not always obeyed especially at high concentrations, but also because of the presence of instrument effects such as the lack of proportionality between the camera signal and the incident radiation intensity and a wavelength range over which the camera integrated instead of a single wavelength. Following Buijs et al. (14), we propose a power law series to take the effects of concentration, instrument effects, as well as surrounding effects into account in a lumped fashion:

$$A = a_1 C + a_2 C^2 + a_3 C^3 + ... + a_n C^n \tag{4}$$

EXPERIMENTAL SETUP

The experimental setup is schematically depicted in Fig.1. An anodized aluminum slab (0.15x0.30x0.02 m) has been used as an IR source. A pseudo-2D sapphire column (0.04x0.2x0.005 m) was installed in front of the IR source. The

2D column allows IR measurements (sapphire being almost transparent to the relevant IR signals). Wall absorbance and reflection were minimized by using a sapphire glass with small thickness (3 mm) and polished surfaces. A porous metal plate with an average pore size of 10 µm and 3 mm thick was used as the gas distributor at the bottom. A nozzle (4 mm inner diameter) was used in the centre of the distributor for CO_2 injection. A high speed IR camera FLIR of 512 x 640 px allowing a maximum full frame rate of 100 frames/s was used to detect transmitted IR radiation. An optical CO_2 filter with a narrow band pass (4.26 ± 0.03 µm) has been used with the camera for CO_2 detection. The camera was positioned at a proper distance and orientation to be able to capture the interested area of the target column and to avoid camera self-reflection, causing the narcissus effect. The wavelength operation of the IR camera allows CO_2 to be detected at 4.26 ± 0.03µm.

To inject CO_2, a piston with adjustable volume has been used that allows fast injection of a measured amount of CO_2 via a nozzle (d = 4 mm) into the bed. Nitrogen is used as diluting agent in single phase and as fluidizing gas in two phase measurements. For gas-solids measurements the column is filled with glass beads as bed material ($d_{particle}$ = 400 ÷ 600 µm, ρ = 2525 kg/m^3), continuously fluidized by N_2 at minimum fluidization gas velocity. The minimum fluidization gas velocity of 0.206 m/s was measured by the pressure drop method (13). The fluidizing gas is initially dried by adsorbing any possible traces of H_2O on SiO_2. CO_2 is filled in a piston at a certain pre-pressure via a three-way valve (V2 in Fig.1). For fast bubble injection CO_2 inside the piston is compressed by air at high pressure (6 bar) and subsequently released into the column through a solenoid valve (Vs), opened in 0.01s. The amount of CO_2 injected is determined by the different pressure before and after injection and the volume of CO_2 filled to the pistol. The injection velocity depends on the amount of tracer gas and the injection time.

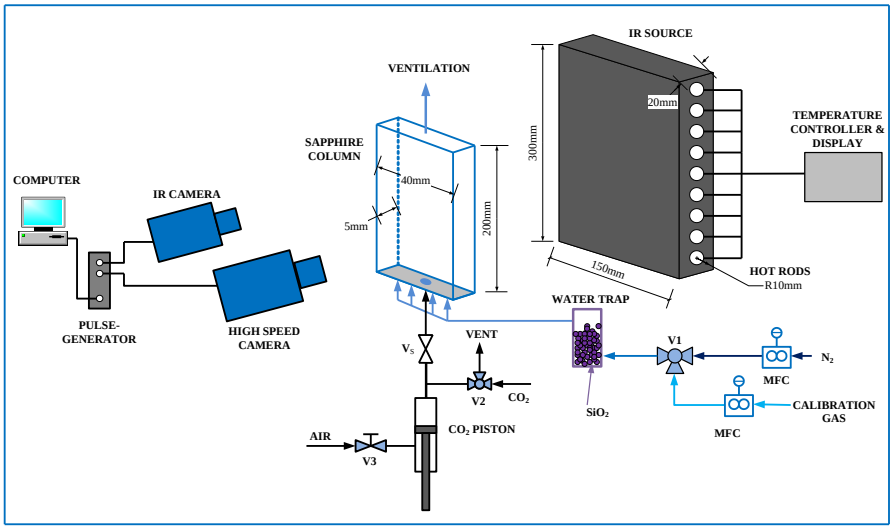

Figure 1: Experimental setup

RESULTS AND DISCUSSION

Calibration procedure

The calibration procedure is carried out by feeding a series of CO_2/N_2 gas mixtures to the sapphire column and recording IR images. Due to the very narrow bandwidth of the filter inside the camera, only CO_2 is detected. The concentration of CO_2 is varied from 0 to 100 % volume at ambient conditions (0 to 0.042 mol/l). Fig. 2 (a) shows the measured average absorbance (averaged over all pixel since the absorbance was quite uniform) as a function of the CO_2 concentration inside the column. The graph shows that at low CO_2 concentrations (0 to 0.01 mol/l), the correlation is approximately linear as described by the Lambert Beer eqn. (Eqn. 4); but non-linear correlation is obtained at higher concentrations. For the studied range of concentrations, a third order correlation well describes the experimental data (Eqn.5).

$$A= a_1C+a_2C^2+a_3C^3 \qquad (5)$$

where a_1, a_2 and a_3 are three fit parameters (a_1 = 39.54 [l/mol], a_2 = -1087 [l^2/mol^2], a_3 = 11805 [l^3/mol^3], R^2= 0.9972).

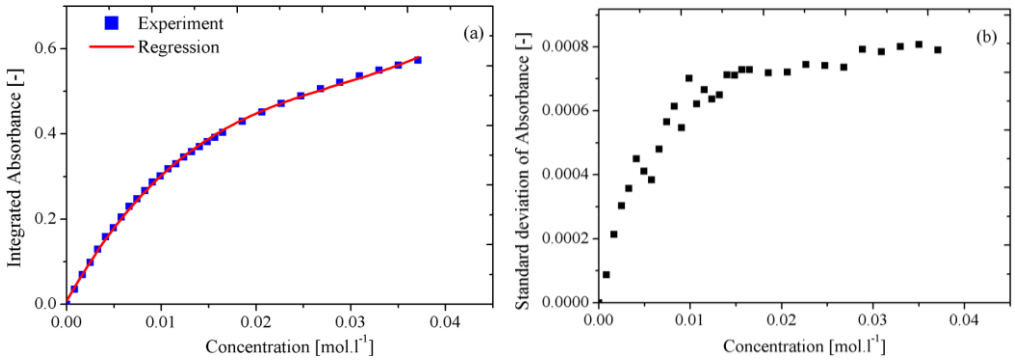

Figure 2: Integrated absorbance (a) and standard deviation of absorbance (b) as a function of tracer gas

In Fig.2 (b), the standard deviation of integrated absorbance is plotted as a function of CO_2 concentration. It shows that the fluctuation of absorbance is increased with the increased concentration. However, the value is not too low (the highest value of the standard deviation is about 0.0008) which again illustrates the uniform absorbance.

Coupled Infrared camera and Digital Image Analysis

The extension of the IR transmission technique to gas-solid flows would make it possible to measure non-invasively concentration profiles inside bubbles rising in gas-solid fluidized beds, giving important information on the bubble-to-emulsion gas exchange rate to be compared with literature findings.

The main difficulty in extending the technique to bubbling fluidized beds is represented by the presence of particles which partly reflect and scatter the IR radiation. These result in the lower signals in the particle positions. Moreover, as bubbles rise in the bed, particles are raining from the roof of the bubbles into the bubble it-self. As the IR technique is only able to detect changes in the camera signal, the presence of particles in the bubbles would lead to erroneous concentration profiles, when not properly corrected for. To avoid this, a visual high speed camera (VIS-2016 x 2016 px @1600Hz from Lavision) is coupled with the IR camera via a pulse generator that sends a trigger to both IR and VIS cameras, for taking coupled IR/VIS images simultaneously. Subsequently, Digital

Image Analysis (DIA) is applied to remove particles inside bubbles before correlating the IR signal to the CO_2 concentration. The DIA script (by applying MATLAB processing tool box) starts by importing both the VIS and IR images. Due to the slightly different angles of both cameras relative to the column, the VIS image is firstly aligned to the same direction of the IR image. Fig.3 shows all steps of the coupling VIS-IR-DIA with the VIS image in Fig.3 (a). The positions of particles inside the bubble and in the emulsion phase can easily be detected from the visual images based on the particle pixel intensity and translated into the binary image (black and white) in which the white colour presents the particles and the black colour for the gas phase (Fig.3 (b)). Subsequently, the particle detection image is overlapped with the IR image (Fig.3(c)) to identify the particles in the IR image The pixel intensity in the IR image, at the positions where particles are present, are replaced by zero intensity. The IR image after removal of the particles (Fig.3 (d)) contains only gas phase which is used to compute the concentration profile, by applying the calibration curve developed in section 4.1. Fig.3 (e) and (f) present the absorbance and concentration profile inside the bubble.

The next step in the DIA technique is to average the concentration inside the whole bubble as well as to determine the equivalent bubble diameter. The snapshots of concentration profiles (Fig.3e) show some dark “spots” caused by the presence of some particles inside the bubble, which will not be taken into account when determining the averaged concentration.

The IR image after removal of particles contains only bubble phase with high signal intensity. The total area of bubble A_b is easily calculated by counting the number of pixels with a high signal intensity. The equivalent bubble diameter is subsequently determined by Eqn. (6):

$$d_b = \sqrt{\frac{4A_b}{\pi}} \qquad (6)$$

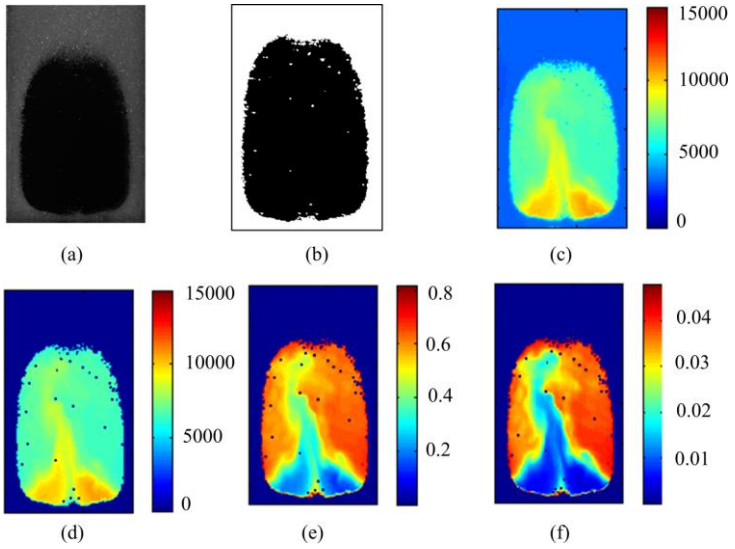

Figure 3: Coupled IR-VIS-DIA procedures: VIS image(a), Particle detection(b), IR image (c), particle removal (d), Absorbance (e) and concentration profile (d)

Gas exchange from bubble-to-emulsion phase in gas-solids fluidized bed

Fig.4 shows snapshots of the tracer gas concentration profiles inside the bubble at different moments in time after injection of a CO_2 bubble into the fluidized bed at minimum fluidization conditions with N_2 as background fluidizing agent. At t= 0.01s, a certain amount of tracer gas is released into the fluidized bed with a nozzle velocity of 17 $m.s^{-1}$, creating a single bubble with high CO_2 concentration. with flat shape at the bottom, due to the effect of the gas distributor.
During the injection, N_2 background fluidization gas enters the bubble and dilutes the CO_2 inside the bubble. The bubble is subsequently growing and rising through the bed, while exchanging gas with the emulsion phase. The concentration field of tracer gas inside the bubble shown in Fig.4 indicates that the mass transport of gas is dominated by convection of fluidization gas rather than diffusion, as expected for the used particle type and size. It is clear that the tracer gas concentration inside the bubble is non-uniform, which is lower in the lower part and in the centre of the bubble. It indicates that the CO_2 in the centre part of the bubble is quickly exchanged with the gas from the emulsion phase, but significant amount of CO_2 is remained in the centre of the vortices at the left and right sides of the bubble. This finding is in good agreement with CFD simulations performed by Patil et al. (6).

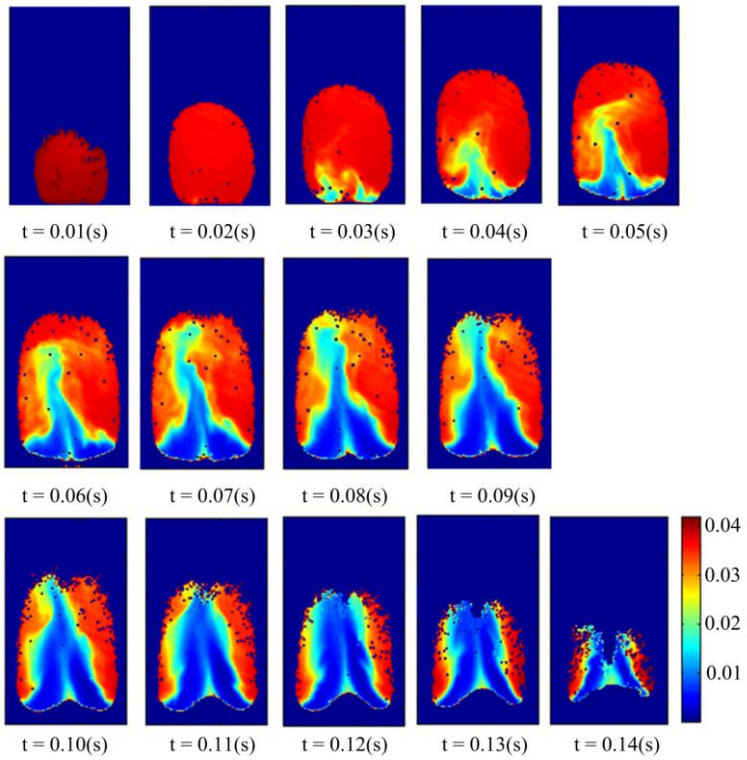

Figure 4: Concentration profile of a single bubble while rising along the bed

Bubble-to-emulsion phase mass transfer coefficient

The averaged CO_2 concentration inside the bubble and the equivalent bubble diameter as function of time are shown in Fig. 5 (a) and (b), respectively. As explained above, the concentration inside the bubble decreases in time, due to the mass exchange with gas in the emulsion phase. At the same time, the bubble is rising and growing, reaching its maximum size of about 42 mm after about 0.07 s after injection. As can be seen, the concentration curve against time reaches a plateau within 0.13 seconds, indicating that the mass exchange rates decreases after this time. The results indicate that the gas exchange is due to a combination

of effects where first convection takes place and afterwards the diffusion from the vortices to the emulsion.
The bubble-to-emulsion phase mass transfer can be described with a convection term and a diffusion term. The convection term describes the flow pattern of the fluidization gas from the emulsion phase inside the bubble which is dominant for the first part of our experiments. The molecular diffusion of CO_2 from the bubble phase (especially from the vortices) to the dense phase also influences the mass transfer process as discussed by Kunii and Levenspiel (2).

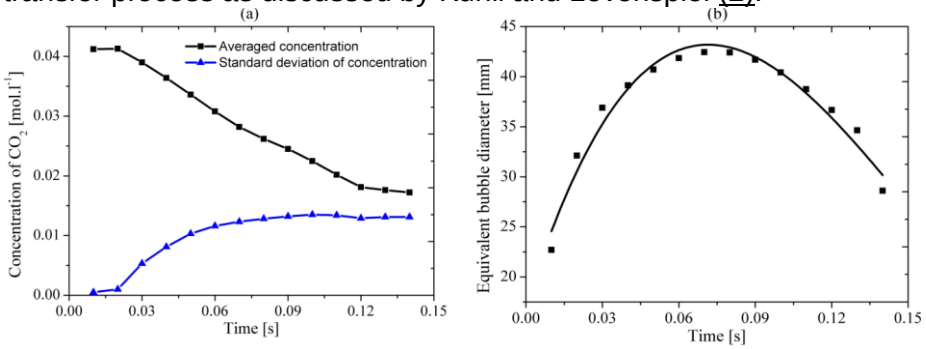

Figure 5: Averaged concentration (a) and equivalent bubble diameter (b) in time.

From the experimental results, the gas exchange rate from bubble to emulsion phase can be estimated by analysing the tracer concentration inside the bubble and solving the mass balance equation for the tracer gas. Assuming that a bubble with initial volume $V_{b,i}$ and with concentration $C_{CO_2,i}$ are generated at the nozzle into a fluidized bed at minimum fluidization conditions with N_2 as fluidizing agent, so that the CO_2 concentration in the emulsion phase remains negligible, the mass balance for the tracer gas reads:

$$\frac{d\left(C_{CO_2,b}V_b\right)}{dt} = -K_{be}(C_{CO_2,b} - C_{CO_2,e})V_b \qquad (7)$$

with initial conditions:

$C_{CO_2,b} = C_{CO_2,i}$ at t = 0

$C_{CO_2,e} = 0$

Integrating Eqn. (7) yields

$$\frac{C_{CO_2,b}(t)\cdot V_b(t)}{C_{CO_2,i}\cdot V_b,i} = \exp\left(-K_{be}t\right) \qquad (8)$$

Because a pseudo-2D bed is used in this work, Eqn. (10) can be written as

$$\frac{C_{CO_2,b}(t)}{C_{CO_2,i}}\left(\frac{D_b(t)}{D_{b,i}}\right)^2 = \exp\left(-K_{be}\times t\right) \qquad (9)$$

From the experiments the averaged CO_2 concentration in the bubble $C_{CO_2,b}$ and the equivalent bubble diameter D_b (Fig.5 a and b) have been determined and fitted as a function of time. By subsequently plotting $\ln\left(\frac{C_{CO_2,b}(t)}{C_{CO_2,i}}\left(\frac{D_b(t)}{D_b,i}\right)^2\right)$ as a

function of time the mass transfer coefficient K_{be} in Eqn. (9) can be calculated from the slope of the curve which yields to the K_{be} of 12.29 s^{-1}.

CONCLUSIONS

A novel optical technique, using a IR and VIS high speed cameras, has been developed to measure CO_2 concentrations in gas and gas-solid flows. The new technique is non-invasive and allows a whole-field virtually instantaneous measurement of the CO_2 concentration with high temporal and spatial resolution. The technique has been calibrated in single phase systems and the calibration has been verified with different calibration mixtures, resulting in relative errors lower than 0.5%. The application of the technique has been subsequently extended to gas-solid bubbling fluidized beds to determine the CO_2 concentration inside the bubbles. A single bubble of CO_2 has been injected into a fluidized bed at minimum fluidization conditions with N_2 as fluidizing agent. In contrast to the assumptions often used in theory and semi-empirical correlations, experiments have shown that the concentration inside the bubble is not uniform and the mass exchange is firstly controlled by convection and afterwards controlled by diffusion between the vortices at the right and left side of the bubble and the emulsion phase. A new model for bubble-to-emulsion phase mass transfer is thus required and the developed technique can be used to perform more detailed experiments. Moreover, the new technique allows ultra-fast and precise measurements that can be applied for studying gas mixing and mass exchange in fluidized beds operated in both bubbling and turbulent regimes.

AKNOWLEDGEMENTS

The authors thank STW for their financial support of this project under the VIDI grant STW10244.

REFERENCES

1. Davidson, J.F., Harrison D., (1963), Cambridge University Press.
2 Kunii, D., Levenspiel, O., (1969), Willey, New York.
3. Murray, J,D., (1963), Harvard Unv.
4. Li, J., Weistein, H.,(1989). *Chem. Eng. Sci.*, 44 (1697-1705).
5. Nguyen, H.V., Potter, O.E., Dent D.C. and Whitehead, A.B., (1981) *AIChE J.*, 27 (509-514).
6. Patil, D.J., van Sint Annaland, M., Kuipers, J.A.M., (2003). *Int. J. Chem. Reac. Eng.* 1.
7. Desmuskh, S., sint Annaland, M., Kuipers, J.A.M (2004). Ind.Eng.Chem.Res.
8. Roels, S., Carmeliet, J.,(2006). Int. J. of Heat & Mass Trans. 49 (2006) 4762–4772.
9. Muller, C.R., Holland, A.J., Gladden, L.F., Davidson J.F., (2008) Powder Technology 183 (53-62)
10. Pavlin T., Wang, R., McGorty, R., Rosen, M.S., Mair, R.W., Walsworth., (2007) App. Mag. Res. 32 (93-112)
11. Chiba, T., Kobayashi, H., Chem.Eng.Sci.(1970).
12. Bauman, P.R., Absorption spectroscopy, Willey, New York (1962).
13. Dang, T.Y.N., Gallucci, F., van Sint Annaland, M., (2013) *submitted to Ind.Eng.Che.Res*.
14. Buijs, K., Maurice M.J., (1969), *Anal. Chim. Acta*, 47(3) (469-474).